Terahertz complex conductivity of nanofibrillar cellulose-PEDOT:PSS composite films

Unuma, Takeya; Kobayashi, Omou; A. Hamdany, Iffah F.; Kumar, Vinay; Saarinen, Jarkko

Published in:
Cellulose

DOI:
10.1007/s10570-019-02276-5

Published: 01/01/2019

Document Version
Accepted author manuscript

Document License
Publisher rights policy

Noname manuscript No.
(will be inserted by the editor)

Terahertz complex conductivity of nanofibrillar cellulose-PEDOT:PSS composite films

Takeya Unuma · Omou Kobayashi · Iffah F. A. Hamdany · Vinay Kumar · Jarkko J. Saarinen

Received: date / Accepted: date

Abstract We investigate the terahertz transmission through flexible composite films that contain nanofibrillar cellulose (NFC) and different blending percentages of the conductive polymer poly(3,4-ethylenedioxythiophene):poly(styrene sulfonate) (PEDOT:PSS). The real part of terahertz complex conductivity is found to decrease with decreasing frequency for each NFC composite film and to approach a finite positive value dependent on the PEDOT:PSS blending percentage in the limit of zero frequency. Both the real and imaginary parts of complex conductivity spectra can be fitted simultaneously with an extended Drude model that describes a partially localized nature of carriers. Our spectral analysis indicates that carriers in the NFC composite become denser and also less localized as the PEDOT:PSS blending percentage is increased.

T. Unuma, O. Kobayashi, and I. F. A. Hamdany
Department of Electrical, Electronics and Information Engineering, Nagaoka University of Technology, Nagaoka, Niigata 940-2188, Japan
E-mail: unuma@vos.nagaokaut.ac.jp

V. Kumar
High Performance Fiber Products, VTT Technical Research Centre of Finland Ltd., FI-02044 VTT, Espoo, Finland

J. J. Saarinen
Department of Chemistry, University of Eastern Finland, Yliopistokatu 7, FI-80130 Joensuu, Finland
E-mail: jarkko.j.saarinen@uef.fi

Graphical abstract

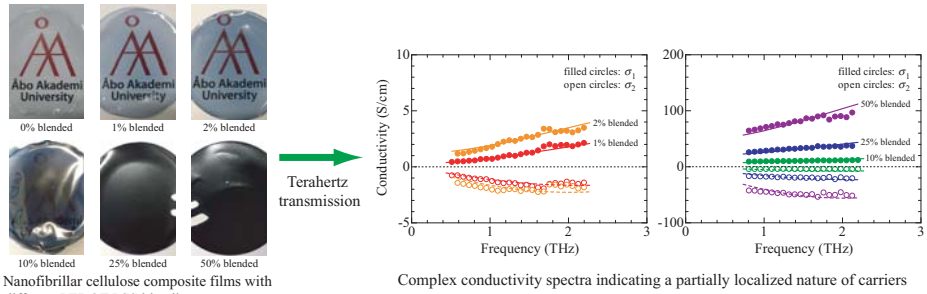

Nanofibrillar cellulose composite films with different PEDOT:PSS blending percentages

Complex conductivity spectra indicating a partially localized nature of carriers

Keywords Nanofibrillar cellulose · Conducting polymers · Composite films · Terahertz spectroscopy · Charge transport

1 Introduction

Nanofibrillar cellulose (NFC) is a promising material owing to its useful properties such as optical transparency, high aspect ratio, mechanical flexibility and strength, small surface roughness, and environmental sustainability (Eichhorn et al. 2010; Klemm et al. 2011; Isogai et al. 2011; Moon et al. 2011; Dufresne 2013). Recently, NFC has been intensively functionalized for organic optoelectronics applications by coating NFC surfaces with conductive materials (Hu et al. 2013; Huang et al. 2013; Penttilä et al. 2013; Wang et al. 2014; Jung et al. 2015; Valtakari et al. 2015) or incorporating them into NFC matrices (van den Berg et al. 2007; Nyström et al. 2010; Müller et al. 2011; Torvinen et al. 2012; Koga et al. 2013; Salajkova et al. 2013; Aleshin et al. 2015; Khan et al. 2015) to provide dc conductivity (Tobjörk and Österbacka 2011; Nyholm et al. 2011). These types of conductive NFC structures have been successfully applied to flexible solar cells (Hu et al. 2013; Nogi et al. 2015), transistors (Huang et al. 2013; Fujisaki et al. 2014), sensors (Koga et al. 2013), and microwave integrated circuits (Jung et al. 2015).

Terahertz (THz) time-domain spectroscopy is a powerful tool for investigating carrier dynamics in semiconductors and biomolecules at frequencies (typically 0.1–10 THz) that characterize the intermixing between electronics and photonics (Ferguson and Zhang 2002; Lloyd-Hughes and Jeon 2012). So far, only a few reports have been published on the THz response of cellulose-based nanomaterials (Andrianov et al. 2015; Carnio et al. 2016; Elfwing et al. 2018), including a conductive composite of bacterial cellulose and poly(3,4-ethylenedioxythiophene):poly(styrene sulfonate) (PEDOT:PSS) (Andrianov et al. 2015). Nevertheless, it is not well understood how the optoelectronic nature of carriers induced by conductive materials can be controlled in NFC composites.

In this paper, we report an observation of the THz transmission through flexible composite films that contained NFC and systematically varied blending percentages of the conductive polymer PEDOT:PSS. The real parts of THz complex

conductivity $\tilde{\sigma}(\omega)$ were found to decrease toward finite positive values (dependent on the PEDOT:PSS blending percentages) with decreasing frequency $\omega/2\pi$, indicating a partially localized nature of carriers in the NFC composite. The real and imaginary parts of $\tilde{\sigma}(\omega)$ were reproduced simultaneously by an extended Drude model with three adjustable parameters. We have shown that carriers in the NFC composite become denser and also less localized as the PEDOT:PSS blending percentage is increased up to 50%.

2 Materials and methods

The samples in our experiment were free-standing NFC composite films with different PEDOT:PSS blending percentages, as listed in Table 1. We prepared composite dispersions in water, blending a PEDOT:PSS dispersion (Clevios PH 500, Heraeus Holding, Germany) in six different dry weight percentages (0–50%) with a hardwood NFC dispersion at a solids content of 2.5% (Bleached Eucalyptus Kraft Pulp, Votorantim Cellulose e Papel, Brazil) received from South China University of Technology. We fabricated the samples by casting the composite dispersions on polystyrene Petri dishes (with a diameter of 8.5 cm) in a controlled atmosphere (temperature: 23°C, relative humidity: 50%) and by lifting the dry films off the dishes. The samples had thicknesses of d = 19–27 μm (see Table 1) in the parts used for THz transmission measurements.

The photographs of the samples taken against a logo mark are shown in Fig. 1, together with the optical transmittance spectra obtained using a UV/Vis/NIR spectrometer (Lambda 900, Perkin Elmer, USA) in the wavelength range of 200–900 nm. Optical transparency was the highest for the 0% blended sample (with transmittance more than 0.9 at visible wavelengths); it decreased gradually as the PEDOT:PSS blending percentage was increased up to 50%. The dc conductivity of the 50% blended sample was estimated to be 45 S/cm at 298 K by the four-probe method.

We measured the THz transmission through the samples at 298 K by using THz time-domain spectroscopy. The measurement system was similar to those reported previously for investigations into the charge transport of doped conjugated polymers including PEDOT:PSS (Unuma et al. 2010, 2013b, 2013a). The THz waves were emitted from a photoconductive antenna modulated at 10 kHz and detected with a ZnTe electro-optic sensor for the 100-ms time constant of a lock-in amplifier, being triggered by 65-fs-long optical pulses delivered from a mode-locked Ti:sapphire laser (Mai Tai SP, Spectra-Physics, USA). All paths of the THz waves were purged with dry air to minimize water vapor, which has

Table 1 PEDOT:PSS blending percentages and film thicknesses of NFC composite samples.

Sample	Film thickness (μm)
0% blended	19
1% blended	23
2% blended	22
10% blended	21
25% blended	27
50% blended	26

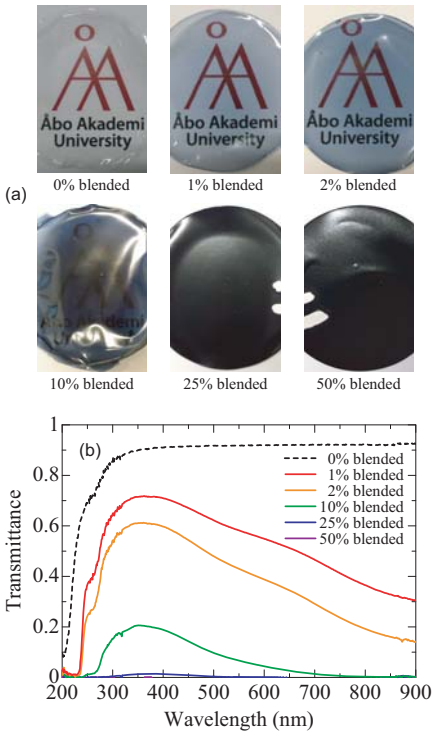

Fig. 1 (a) Photographs and (b) optical transmittance spectra of NFC composite samples with different PEDOT:PSS blending percentages of 0–50%.

strong absorption particularly at 1.7 THz and gives rise to spectral distortion. We obtained the complex conductivity spectra $\tilde{\sigma}(\omega) = \sigma_1(\omega) + i\sigma_2(\omega)$ of the 1–50% blended samples, where the real part $\sigma_1(\omega)$ and the minus imaginary part $-\sigma_2(\omega)$ describe the conductive and dielectric properties of carriers at frequency $\omega/2\pi$, respectively.

3 Results and discussion

The temporal waveforms of THz electric fields transmitted through the samples are shown in Fig. 2, together with that passing through the sample space for reference. We found two pronounced features, on which the current extent of thickness variation (see Table 1) had minor effects qualitatively, in these THz waveforms. First, the THz signals appeared with systematic shifts in time, indicating that the velocity c/n of the THz waves (c: vacuum light velocity, n: refractive index) inside the NFC composite decreased significantly as the PEDOT:PSS blending percentage was increased. Second, the amplitude decreased substantially with the PEDOT:PSS blending percentage, suggesting an increase in the absorption coefficient α of the NFC composite.

Performing the Fourier transformation of the observed THz waveforms, we obtained the complex transmission coefficient spectra $\tilde{t}(\omega)$ of the samples. The

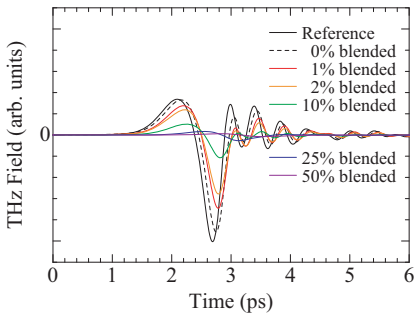

Fig. 2 Temporal waveforms of THz electric fields transmitted through NFC composite samples, having larger phase delays and smaller amplitudes for higher PEDOT:PSS blending percentages. The time origin ($t = 0$) is set to an arbitrary position.

complex refractive index spectra $\tilde{n}(\omega) = n(\omega) + i\kappa(\omega)$, whose imaginary parts are the extinction coefficient spectra associated with the absorption coefficient spectra via $\alpha(\omega) = 2\omega\kappa(\omega)/c$, are linked to $\tilde{t}(\omega)$ as given by (Unuma et al. 2010, 2013b)

$$\tilde{t} = \frac{4\tilde{n}}{(\tilde{n}+1)^2} e^{i\omega(\tilde{n}-1)d/c} \sum_l \left(\frac{\tilde{n}-1}{\tilde{n}+1}\right)^{2l} e^{i\omega 2l\tilde{n}d/c}, \quad (1)$$

where l $(= 0, 1, 2, \cdots)$ is the integer numbering a pair of internal reflections on the back and front surfaces of the NFC composite. The inclusion of multiple reflections with $0 \leq l \leq 5$ in Eq. (1) was sufficient to find the proper numerical solution for $\tilde{n}$ at each ω because the THz waves were significantly damped by absorption during the multiple reflections. The complex conductivity spectra $\tilde{\sigma}(\omega) = \sigma_1(\omega) + i\sigma_2(\omega)$ for carriers induced by PEDOT:PSS are expressed as $\sigma_1 = 2\omega\epsilon_0 n\kappa$ and $\sigma_2 = \omega\epsilon_0(\kappa^2 - n^2 + \varepsilon_\infty)$, with ϵ_0 being the vacuum permittivity and ε_∞ being the high-frequency background dielectric constant (Unuma et al. 2010, 2013b). The pristine NFC, i.e., 0% blended sample, exhibited almost constant refractive indices of 1.8–1.9 and sufficiently small extinction coefficients at frequencies of up to ~ 3 THz, suggesting that ε_∞ can be set to 3.3 for a crude approximation. Thus, we were able to determine $\tilde{\sigma}(\omega)$ for carriers in the NFC composite.

Figure 3 shows the complex conductivity spectra $\tilde{\sigma}(\omega)$ of the 1–50% blended samples. Both the real parts σ_1 (filled circles) and the imaginary parts σ_2 (open circles) are larger for higher PEDOT:PSS blending percentages. Note that the values of σ_1 observed for the 10%, 25%, and 50% blended samples are one or two orders of magnitude larger than those reported previously for a PEDOT:PSS blended bacterial cellulose film ($\sigma_1 \sim 1$ S/cm) (Andrianov et al. 2015). For each sample, σ_1 gradually decreased toward a finite positive value with decreasing frequency $\omega/2\pi$, while the imaginary part σ_2 remained negative. These spectral features are similar to those reported for doped polythiophenes (including PEDOT:PSS) (Unuma et al. 2010), meaning that carriers in the NFC composite have a partially localized nature.

We performed a detailed spectral analysis of $\tilde{\sigma}(\omega)$ by adopting the Drude-Smith model (Smith 2001), which has been widely used to describe the optoelectronic response of partially localized carriers in nanoparticle composites (Turner et al.

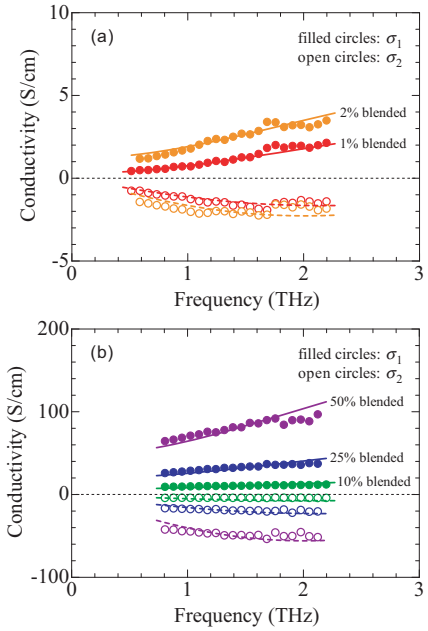

Fig. 3 THz complex conductivity spectra $\tilde{\sigma}(\omega)$ of NFC composite samples, having larger values for higher PEDOT:PSS blending percentages. Fits of the Drude-Smith model to $\tilde{\sigma}(\omega)$ are shown by curves.

2002; Baxter and Schmuttenmaer 2006; Cooke et al. 2006; Walther et al. 2007) and conjugated polymers (Ai et al. 2006; Cunningham and Hayden 2008; Unuma et al. 2010; Cooke et al. 2012; Unuma et al. 2013b, 2013a). The complex conductivity in the Drude-Smith model is expressed as (Smith 2001)

$$\tilde{\sigma}_{\mathrm{DS}}(\omega) = \frac{Ne^2\tau/m^*}{1-i\omega\tau}\left(1+\frac{C}{1-i\omega\tau}\right), \tag{2}$$

where N is the volume density of carriers, τ is the momentum relaxation time, m^* is the effective mass, and C is the localization degree that can change from -1 (for completely localized carriers) to 0 (for free carriers in the Drude model). The carriers induced by PEDOT:PSS are supposed to be positive polarons (Furukawa 1996) and theoretically to have an effective mass of nearly $2m_0$ with m_0 being the vacuum electron mass (Lee et al. 1993). In our spectral analysis, we adopted an experimental value of $m^* = 1.7m_0$ estimated previously by optical reflection spectroscopy (Lee et al. 1995). Treating N, C, and τ as adjustable parameters, we fitted Eq. (2) to the observed complex conductivity spectra $\tilde{\sigma}(\omega)$.

The fits to $\tilde{\sigma}(\omega)$ for the 1–50% blended samples are shown in Fig. 3 by curves, and the corresponding sets of fitting parameters N, C, and τ are shown in Fig. 4 by symbols. As seen in Fig. 3, the observed spectral features of σ_1 and σ_2 are reproduced simultaneously by the DS model for each sample. When the fit for the 50% blended sample is extrapolated to lower frequencies, it gives $\tilde{\sigma}_{\mathrm{DS}}(0) = 47$ S/cm in reasonable agreement with the four-probe measurement of dc conductivity

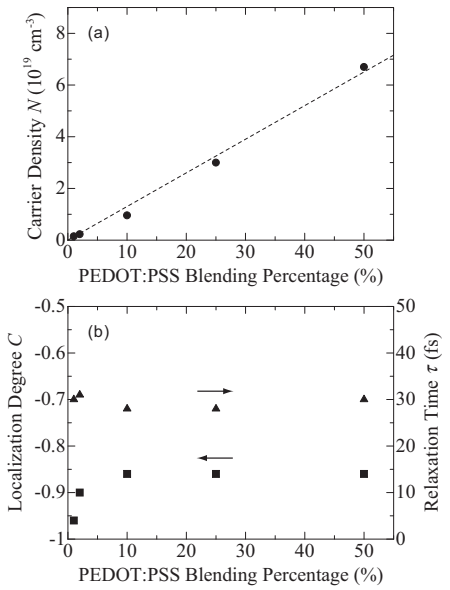

Fig. 4 Carrier density N (circles), localization degree C (squares), and relaxation time τ (triangles) plotted versus PEDOT:PSS blending percentage for NFC composite samples. The dashed line in (a) shows a linear regression.

(45 S/cm) mentioned earlier. Thus, the Drude-Smith model covers the dc-to-THz charge transport in the NFC composite. Figure 4 reveals that carrier density N increased monotonically from 1.5×10^{18} to 6.7×10^{19} cm^{-3}, localization degree C varied from -0.96 to -0.86 and was then saturated, and relaxation time τ was kept almost constant at 30 fs with an increase in the PEDOT:PSS blending percentage up to 50%.

Now, let us discuss a possible reason for this behavior of the three fitting parameters. Carrier density N is expected to express the number of carriers in PEDOT:PSS divided by the total volume of the NFC composite. Hence, N should increase in proportion to the PEDOT:PSS blending percentage. A linear regression (dashed line) indeed applies well to the data points for N (circles) in Fig. 4(a). On the other hand, localization degree C and relaxation time τ are expected to be governed by conduction paths (Unuma et al. 2010, 2013b, 2013a) in the NFC composite. The values of C and τ for the 10–50% blended samples can be regarded as taking over the original nature of carriers inherent in PEDOT:PSS because similar values have also been observed for doped conjugated polymers themselves (Unuma et al. 2010, 2013b, 2013a). Conduction paths for much lower PEDOT:PSS blending percentages may well be rather separated from each other, e.g., owing to the coagulation or adsorption of PEDOT:PSS onto NFC fibrils, and can exhibit stronger localization of carriers (C nearer to -1).

4 Conclusion

We measured the THz complex conductivity spectra $\tilde{\sigma}(\omega)$ of NFC composite films with different PEDOT:PSS blending percentages. The real parts of $\tilde{\sigma}(\omega)$ decreased toward finite positive values (dependent on the PEDOT:PSS blending percentages) with decreasing frequency $\omega/2\pi$, while the imaginary parts of $\tilde{\sigma}(\omega)$ remained negative. These spectral features indicate that carriers in the NFC composite have a partially localized nature. The real and imaginary parts of $\tilde{\sigma}(\omega)$ were fitted simultaneously with the Drude-Smith model. From the behavior of fitting parameters, we found that carriers in the NFC composite become denser and also less localized as the PEDOT:PSS blending percentage is increased up to 50%. Thus, we have provided an essential insight into how the optoelectronic nature of carriers in NFC composites can be controlled with conductive materials, demonstrating potential usefulness of NFC composites in the THz region.

Acknowledgements This work was partly supported by a Nagaoka University of Technology Presidential Research Grant. J. J. S. wishes to thank the UEF Faculty of Science and Forestry (Grant No. 579/2017) for the financial support. Åbo Akademi University (Laboratory of Paper Coating and Converting) and South China University of Technology (State Key Laboratory of Pulp and Paper Engineering) are acknowledged for laboratory access during the sample preparation and for producing NFC suspensions, respectively.

References

Ai X, Beard MC, Knutsen KP, Shaheen SE, Rumbles G, Ellingson RJ (2006) Photoinduced charge carrier generation in a poly(3-hexylthiophene) and methanofullerene bulk heterojunction investigated by time-resolved terahertz spectroscopy. J Phys Chem B 110:25462–25471

Aleshin AN, Berestennikov AS, Krylov PS, Shcherbakov IP, Petrov VN, Trapeznikova IN, Mamalimova RI, Khripunov AK, Tkachenko AA (2015) Electrical and optical properties of bacterial cellulose films modified with conductive polymer PEDOT/PSS. Synth Metals 199:147–151

Andrianov AV, Aleshin AN, Khripunov AK, Trukhin VN (2015) Terahertz properties of bacterial cellulose films and its composite with conducting polymer PEDOT/PSS. Synth Metals 205:201–205

Baxter JB, Schmuttenmaer CA (2006) Conductivity of ZnO nanowires, nanoparticles, and thin films using time-resolved terahertz spectroscopy. J Phys Chem B 110:25229–25239

Carnio BN, Ahvazi B, Elezzabi AY (2016) Terahertz properties of cellulose nanocrystals and films. J Infrared Millim Terahertz Waves 37:281–288

Cooke DG, Krebs FC, Jepsen PU (2012) Direct observation of sub-100 fs mobile charge generation in a polymer-fullerene film. Phys Rev Lett 108:056603

Cooke DG, MacDonald AN, Hryciw A, Wang J, Li Q, Meldrum A, Hegmann FA (2006) Transient terahertz conductivity in photoexcited silicon nanocrystal films. Phys Rev B 73:193311

Cunningham PD, Hayden LM (2008) Carrier dynamics resulting from above and below gap excitation of P3HT and P3HT/PCBM investigated by optical-pump terahertz-probe spectroscopy. J Phys Chem C 112:7928–7935

Dufresne A (2013) Nanocellulose: a new ageless bionanomaterial. Mat Today 16:220–227

Eichhorn SJ, Dufresne A, Aranguren M, Marcovich NE, Capadona JR, Rowan SJ, Weder C, Thielemans W, Roman M, Renneckar S, Gindl W, Veigel S, Keckes J, Yano H, Abe K, Nogi M, Nakagaito AN, Mangalam A, Simonsen J, Benight AS, Bismarck A, Berglund LA, Peijs T (2010) Review: current international research into cellulose nanofibres and nanocomposites. J Mater Sci 45:1–33

Elfwing A, Ponseca Jr CS, Ouyang L, Urbanowicz A, Krotkus A, Tu D, Forchheimer R, Inganäs O (2018) Conducting helical structures from celery decorated with a metallic conjugated polymer give resonances in the terahertz range. Adv Funct Mater 28:1706595

Ferguson B, Zhang X-C (2002) Materials for terahertz science and technology. Nat Mater 1:26–33

Fujisaki Y, Koga H, Nakajima Y, Nakata M, Tsuji H, Yamamoto T, Kurita T, Nogi M, Shimidzu N (2014) Transparent nanopaper-based flexible organic thin-film transistor array. Adv Funct Mater 24:1657–1663

Furukawa Y (1996) Electronic absorption and vibrational spectroscopies of conjugated conducting polymers. J Phys Chem 100:15644–15653

Hu L, Zheng G, Yao J, Liu N, Weil B, Eskilsson M, Karabulut E, Ruan Z, Fan S, Bloking JT, McGehee MD, Wagberg L, Cui Y (2013) Transparent and conductive paper from nanocellulose fibers. Energy Environ Sci 6:513–518

Huang J, Zhu H, Chen Y, Preston C, Rohrbach K, Cumings J, Hu L (2013) Highly transparent and flexible nanopaper transistors. ACS Nano 7:2106–2113

Isogai A, Saito T, Fukuzumi H (2011) TEMPO-oxidized cellulose nanofibers. Nanoscale 3:71–85

Jung YH, Chang T-H, Zhang H, Yao C, Zheng Q, Yang VW, Mi H, Kim M, Cho SJ, Park D-W, Jiang H, Lee J, Qiu Y, Zhou W, Cai Z, Gong S, Ma Z (2015) High-performance green flexible electronics based on biodegradable cellulose nanofibril paper. Nat Commun 6:7170

Khan S, Ul-Islam M, Khattak WA, Ullah MW, Park JK (2015) Bacterial cellulose-poly(3,4-ethylenedioxythiophene)-poly(styrenesulfonate) composites for optoelectronic applications. Carbohydr Polym 127:86–93

Klemm D, Kramer F, Moritz S, Lindström T, Ankerfors M, Gray D, Dorris A (2011) Nanocelluloses: a new family of nature-based materials. Angew Chem Int Ed 50:5438–5466

Koga H, Saito T, Kitaoka T, Nogi M, Suganuma K, Isogai A (2013) Transparent, conductive, and printable composites consisting of TEMPO-oxidized nanocellulose and carbon nanotube. Biomacromolecules 14:1160–1165

Lee K, Heeger AJ, and Cao Y (1993) Reflectance of polyaniline protonated with camphor sulfonic acid: Disordered metal on the metal-insulator boundary. Phys Rev B 48:14884–14891

Lee K, Menon R, Yoon CO, Heeger AJ (1995) Reflectance of conducting polypyrrole: Observation of the metal-insulator transition driven by disorder. Phys Rev B 52:4779–4787

Lloyd-Hughes J, Jeon T-I (2012) A review of the terahertz conductivity of bulk and nanomaterials. J Infrared Millim Terahertz Waves 33:871–925

Moon RJ, Martini A, Nairn J, Simonsen J, Youngblood J (2011) Cellulose nanomaterials review: structure, properties and nanocomposites. Chem Soc Rev 40:3941–3994

Müller D, Rambo CR, Recouvreux DOS, Porto LM, Barra GMO (2011) Chemical in situ polymerization of polypyrrole on bacterial cellulose nanofibers. Synth Metals 161:106–111

Nogi M, Karakawa M, Komoda N, Yagyu H, Nge TT (2015) Transparent conductive nanofiber paper for foldable solar cells. Sci Rep 5:17254

Nyholm L, Nyström G, Mihranyan A, Strømme M (2011) Toward flexible polymer and paper-based energy storage devices. Adv Mater 23:3751–3769

Nyström G, Mihranyan A, Razaq A, Lindström T, Nyholm L, Strømme M (2010) A nanocellulose polypyrrole composite based on microfibrillated cellulose from wood. J Phys Chem B 114:4178–4182

Penttilä A, Sievänen J, Torvinen K, Ojanperä K, Ketoja JA (2013) Filler-nanocellulose substrate for printed electronics: experiments and model approach to structure and conductivity. Cellulose 20:1413–1424

Salajkova M, Valentini L, Zhou Q, Berglund LA (2013) Tough nanopaper structures based on cellulose nanofibers and carbon nanotubes. Composites Sci Technol 87:103–110

Smith NV (2001) Classical generalization of the Drude formula for the optical conductivity. Phys Rev B 64:155106

Tobjörk D, Österbacka R (2011) Paper electronics. Adv Mater 23:1935–1961

Torvinen K, Sievänen J, Hjelt T, Hellén E (2012) Smooth and flexible filler-nanocellulose composite structure for printed electronics applications. Cellulose 19:821–829

Turner GM, Beard MC, Schmuttenmaer CA (2002) Carrier localization and cooling in dye-sensitized nanocrystalline titanium dioxide. J Phys Chem B 106:11716–11719

Unuma T, Fujii K, Kishida H, Nakamura A (2010) Terahertz complex conductivities of carriers with partial localization in doped polythiophenes. Appl Phys Lett 97:033308

Unuma T, Umemoto A, Kishida H (2013) Anisotropic terahertz complex conductivities in oriented polythiophene films. Appl Phys Lett 103:213305

Unuma T, Yamada N, Nakamura A, Kishida H, Lee S-C, Hong E-Y, Lee S-H, Kwon O-P (2013) Direct observation of carrier delocalization in highly conducting polyaniline. Appl Phys Lett 103:053303

Valtakari D, Liu J, Kumar V, Xu C, Toivakka M, Saarinen JJ (2015) Conductivity of PEDOT:PSS on spin-coated and drop cast nanofibrillar cellulose thin films. Nanoscale Res Lett 10:386

Van den Berg O, Schroeter M, Capadonaac JR, Weder C (2007) Nanocomposites based on cellulose whiskers and (semi)conducting conjugated polymers. J Mater Chem 17:2746–2753

Walther M, Cooke DG, Sherstan C, Hajar M, Freeman MR, Hegmann FA (2007) Terahertz conductivity of thin gold films at the metal-insulator percolation transition. Phys Rev B 76:125408

Wang X, Gao K, Shao Z, Peng X, Wu X, Wang F (2014) Layer-by-layer assembled hybrid multilayer thin film electrodes based on transparent cellulose nanofibers paper for flexible supercapacitors applications. J Power Sources 249:148–155